The Astrophysical Journal, 775:96 (8pp), 2013 October 1 doi:10.1088/0004-637X/775/2/96

THE STRUCTURE OF SURFACE H_2O LAYERS OF ICE-COVERED PLANETS WITH HIGH-PRESSURE ICE

S. Ueta and T. Sasaki
Earth and Planetary Sciences, Tokyo Institute of Technology, 2-12-1 Ookayama, Meguro-ku, Tokyo 152-8551, Japan; ueta@geo.titech.ac.jp, takanori@geo.titech.ac.jp
Received 2012 November 12; accepted 2013 July 30; published 2013 September 11

ABSTRACT

Many extrasolar (bound) terrestrial planets and free-floating (unbound) planets have been discovered. While the existence of bound and unbound terrestrial planets with liquid water is an important question, of particular importance is the question of these planets' habitability. Even for a globally ice-covered planet, geothermal heat from the planetary interior may melt the interior ice, creating an internal ocean covered by an ice shell. In this paper, we discuss the conditions that terrestrial planets must satisfy for such an internal ocean to exist on the timescale of planetary evolution. The question is addressed in terms of planetary mass, distance from a central star, water abundance, and abundance of radiogenic heat sources. In addition, we investigate the structure of the surface H_2O layers of ice-covered planets by considering the effects of ice under high pressure (high-pressure ice). As a fiducial case, a 1 $M_\oplus$ planet at 1 AU from its central star and with 0.6–25 times the H_2O mass of the Earth could have an internal ocean. We find that high-pressure ice layers may appear between the internal ocean and the rock portion on a planet with an H_2O mass over 25 times that of the Earth. The planetary mass and abundance of surface water strongly restrict the conditions under which an extrasolar terrestrial planet may have an internal ocean with no high-pressure ice under the ocean. Such high-pressure ice layers underlying the internal ocean are likely to affect the habitability of the planet.

Key words: astrobiology – planets and satellites: composition – planets and satellites: general – planets and satellites: interiors – planets and satellites: surfaces

1. INTRODUCTION

Since the first extrasolar planet was discovered in 1995 (Mayor & Queloz 1995), more than 800 exoplanets have been detected as of 2013 March, owing to improvements in both observational instruments and analysis methods. Although most known exoplanets are gas giants, estimates based on both theory and observations indicate that terrestrial planets are also common (Howard et al. 2010). Supporting these estimates is the fact that Earth-like planets have indeed been discovered. Moreover, space telescopes (e.g., *Kepler*) have now released observational data about many terrestrial planet candidates. Whether terrestrial planets with liquid water exist is an important question to consider because it lays the groundwork for the consideration of habitability.

The orbital range around a star for which liquid water can exist on a planetary surface is called the habitable zone (HZ; Hart 1979; Kasting et al. 1993). The inner edge of the HZ is determined by the runaway greenhouse limit (Kasting 1988; Nakajima et al. 1992) and the outer edge is estimated from the effects of CO_2 clouds (Kasting et al. 1993; Mischna et al. 2000). The region between these edges is generally called the HZ for terrestrial planets with plentiful liquid water on their surfaces (ocean planets). Planets with plentiful water on the surface but outside the outer edge of the HZ would be globally covered with ice and no liquid water would exist on the surface. These planets are called "snowball planets" (Tajika 2008). Moreover, an ocean planet could be ice-covered even within the HZ because multiple climate modes are possible, including ice-free, partially ice-covered, and globally ice-covered states (Budyko 1969; Sellers 1969; Tajika 2008). Although such planets would be globally ice-covered, liquid water could exist beneath the surface ice shell if sufficient geothermal heat flows up from the planetary interior to melt the interior ice. In this scenario, only a few kilometers of ice would form at the surface of the ocean (Hoffman & Schrag 2002) and life could exist in the liquid water under the surface ice shell (Hoffman et al. 1998; Hoffman & Schrag 2002; Gaidos et al. 1999).

Another possibility is presented by planets that float in space without being gravitationally bound to a star (free-floating planets), as have been found thanks to recent advances in observational techniques (Sumi et al. 2011). Although such planets receive no energy from a central star, even a free-floating Earth-sized planet with considerable geothermal heat could have liquid water under an ice-covered surface.

Considering geothermal heat from the planetary interior, Tajika (2008) discusses the theoretical restrictions for ice-covered extrasolar terrestrial planets that, on the timescale of planetary evolution, have an internal ocean. Tajika (2008) shows that an internal ocean can exist if the water abundance and planetary mass are comparable to those of Earth. A planet with a mass less than 0.4 $M_\oplus$ cannot maintain an internal ocean. For a planet with mass $\geqslant 4\,M_\oplus$, liquid water would be stable either on the planetary surface or under the ice, regardless of the luminosity of the central star and the planetary orbit. These are important conclusions and have important implications for habitable planets.

In this paper, we extend the analysis of Tajika (2008) and vary the parameter values such as the abundance of radiogenic heat sources and the H_2O abundance on the surface. Although Tajika (2008) assumed that the mass ratio of H_2O on the planetary surface is the same as that on Earth (0.023% by weight), the origin of water on the Earth is not apparent (Genda & Ikoma 2008) so it is possible that extrasolar terrestrial planets have some order of the H_2O abundance of Earth. We investigate this possibility by varying the H_2O abundance in our simulations, and also by checking whether ice appears under H_2O layers under high-pressure conditions (see Section 2.2). Therefore, in this

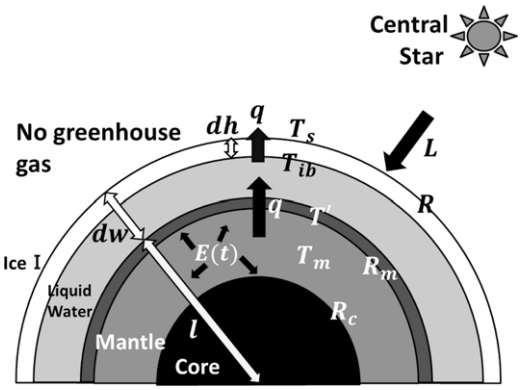

Figure 1. Schematic of the model used in this study.

work, we consider the effect of high-pressure ice under an internal ocean and discuss its implications for habitability (see Section 4.2). With these considerations, we discuss the conditions required for bound and unbound terrestrial planets to have an internal ocean on the timescale of planetary evolution (owing to the geothermal heat flux from the planetary interior). Our discussion further considers various planetary masses, distances from the central star, water abundances, and the abundances of radiogenic heat sources. Finally, we investigate the structure of surface H_2O layers of ice-covered planets by taking into account the effects of high-pressure ice.

2. METHOD

2.1. Numerical Model

To calculate the mass–radius relationships for planets with masses in the range 0.1 $M_\oplus$–10 $M_\oplus$, we adjust the planetary parameters. We assume

$$\frac{R}{R_\oplus} = \left(\frac{M}{M_\oplus}\right)^{0.27}, \tag{1}$$

as per Valencia et al. (2006), where R is the planetary radius and M is the planetary mass. The subscript $\oplus$ denotes values for Earth. The mantle thickness, core size, amount of H_2O, average density, and other planetary properties are scaled according to this equation.

The planetary surfaces are assumed to consist of frozen H_2O and to have no continental crust. We define the planetary radius as $R = dw + l$, where dw is the H_2O thickness and l is the mantle-core radius (see Figure 1). The mass of H_2O on the planetary surface is given by

$$M_{sw} = \frac{4}{3}\pi\rho_w[(dw + l)^3 - l^3], \tag{2}$$

where ρ_w is the density of H_2O. We vary M_{sw} from 0.1 M_{sw0} to 100 M_{sw0}, where $M_{sw0} = 0.00023M$, with the coefficient being the H_2O abundance of Earth (0.023% by weight).

Assuming that a heat flux q is transferred from the planetary interior through the surface ice shell by thermal conduction, the ice thickness dh can be calculated as

$$dh = k_i \frac{T_{ib} - T_s}{q}, \tag{3}$$

where k_i is the thermal conductivity of ice, T_{ib} is the temperature at the bottom of the ice, and T_s is the temperature at the surface.

We assume that the surface ice is hexagonal ice (ice Ih). Between 0.5 K and 273 K, the thermal conductivity of ice Ih is known (Klinger 1975; Varrot et al. 1978). For temperatures greater than ~25 K, the conductivity is given by Klinger (1980) as

$$k_i = \frac{567[\mathrm{Wm}^{-1}]}{T}. \tag{4}$$

To estimate T_{ib}, we assume that the melting line of H_2O is a straight line connecting (0 bar, 273 K) to (2072 bar, 251 K) in the linear pressure–temperature phase diagram. The temperature T_{ib} can be estimated using

$$\begin{aligned} T_{ib} &= 273 - \frac{22[\mathrm{K}]}{2072[\mathrm{bar}]} p_{ib} \\ &= 273 - \frac{22[\mathrm{K}]}{2072[\mathrm{bar}]} dh\rho_w g \times 10^{-5}, \end{aligned} \tag{5}$$

where p_{ib} (bar) is the pressure at the bottom of the ice and g is the gravitational acceleration on Earth.

Considering energy balance on the planetary surface, the planetary surface temperature T_s is

$$\frac{(1-A)}{4d^2}\frac{L}{4\pi D_0^2} + q = \varepsilon\sigma T_s^4, \tag{6}$$

where A is the planetary albedo, d is the distance from the central star in AU, L is the luminosity of the central star, $D_0 = 1.5 \times 10^{11}$ m is a distance of 1 AU in meters, ε is the emissivity of the planet, and $\sigma = 5.67 \times 10^{-8}$ Wm^{-2} K^{-4} is the Stefan–Boltzmann constant. We assume $A = 0.62$ and $\varepsilon = 1.0$ (i.e., the planetary atmosphere contains no greenhouse gases, which yields an upper estimate on the ice thickness). The increase in luminosity due to the evolution of the central star as a main sequence star (Gough 1981) is considered using

$$L(t) = \left[1 + \frac{2}{5}\left(1 - \frac{t}{t_\odot}\right)\right]^{-1} L_\odot, \tag{7}$$

where $t_\odot = 4.7 \times 10^9$ yr and $L_\odot = 3.827 \times 10^{26}$ W.

From these models, we can obtain the H_2O thickness dw and the ice thickness dh. The condition for terrestrial planets having an internal ocean is

$$dw > dh. \tag{8}$$

To estimate the geothermal heat flux q through planetary evolution, we investigate the thermal evolution of terrestrial planets using a parameterized convection model (Tajika & Matsui 1992; McGovern & Schubert 1989; Franck & Bounama 1995; von Bloh et al. 2007; see the Appendix for details). We assume E, which is the initial heat generation per unit time and volume, to be $0.1E_0$–$10E_0$, where the constant E_0 is the initial heat generation estimated from the present heat flux of the Earth (see the Appendix for details).

2.2. High-pressure Ice

Ice undergoes a phase transition at high pressure (Figure 2). Unlike ice Ih, the other phases are more dense than liquid H_2O. We call the denser ice "high-pressure ice." Because Tajika (2008) assumes that the amount of H_2O on the planetary surface is the same as that on the Earth's surface M_{sw0} (= 0.00023M), the only possible conditions on the planetary surface are those labeled 1, 2, and 3 in Figure 3. However, because we consider

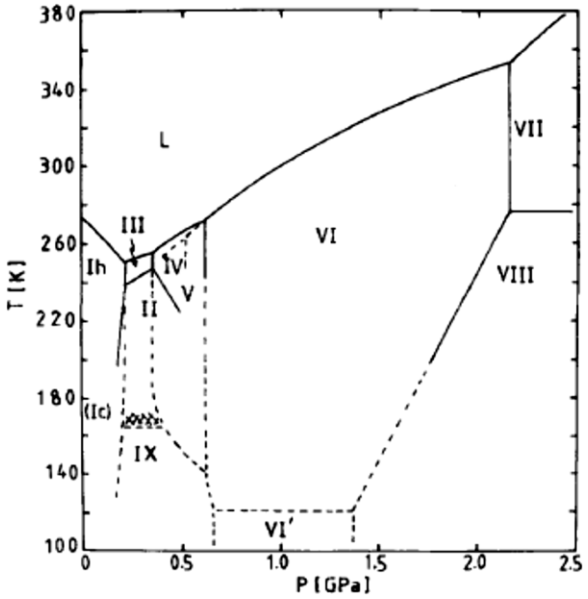

Figure 2. Phase diagram of H_2O (after Kamb 1973).

herein that H_2O mass may range from $0.1\,M_{sw0}$ to $100\,M_{sw0}$, the H_2O–rock boundary could move to higher pressure, so we should account for the effect of high-pressure ice (Figure 3(a)). Therefore, types 4, 5, and 6 of Figure 3(b) are added as possible surface conditions. Type 2 and type 5 planets both have an internal ocean, but high-pressure ice exists in type 5 planets between the internal ocean and the underlying rock.

We approximate the melting curve by straight lines connecting the triple points in the linear pressure–temperature phase diagram. We also assume that the amount of heat flux from the planetary interior that is transferred through the internal ocean by thermal convection is the same as that transferred through the surface ice. Here, we presume that the temperature gradient in the liquid water part of the phase diagram is isothermal (Figures 3(a) and (c)), although a gradient in a deeper internal ocean than what is considered in this study should be carefully discussed. The condition for high-pressure ice to exist under the internal ocean is

$$P_h < P_b, \tag{9}$$

where P_b is the pressure at the H_2O–rock boundary and P_h is the pressure in the phase diagram where the temperature gradient and the high-pressure melting line cross (Figure 3(c)). As a representative value, we assume that high-pressure ice has a density of 1.2 g cm^{-3}. Because the characteristic features of high-pressure ice are poorly understood, we simplified the model and, in particular, the thermal conductivities of the high-pressure ice (see below). When the thermal conductivity of high-pressure ice is relatively high and the temperature gradient in the high-pressure ice part of the phase diagram is shallower than the gradient of the melting lines, the layer of high-pressure ice continues to the H_2O–rock boundary ((i) in Figure 3(c)). However, when the thermal conductivity is comparatively low and the temperature gradient is steeper than that of the melting lines, the temperature gradient joins the melting line and goes along with the melting lines to the H_2O–rock boundary (dashed arrows (ii) and (iii) in Figure 3(c)). Although little is known about the conditions on the dashed arrows, we assume that layer to be high-pressure ice in this study. Therefore, from the point where the temperature–pressure line crosses into the high-pressure ice part, the high-pressure layer continues to the H_2O–rock boundary.

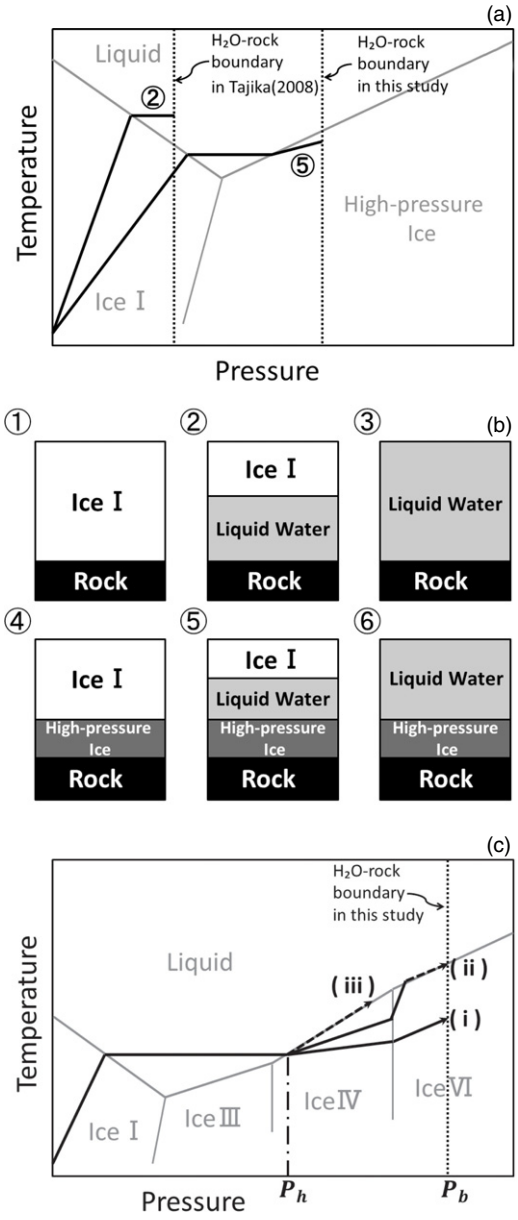

Figure 3. (a) Schematic phase diagram of H_2O (gray lines), temperature gradient (black lines), and H_2O–rock boundaries (dashed lines). (b) Types of planets that have H_2O on their surfaces. (c) Schematic of models used to treat high-pressure ice.

3. RESULTS

Figures 4(a) and (b) show the surface conditions for planets with masses from $0.1\,M_\oplus$ to $10\,M_\oplus$ 4.6 billion yr after planetary formation, with varying H_2O masses on their surfaces or initial radiogenic heat sources. All of the planets are located 1 AU from thier central star. We assumed $E/E_0 = 1$ for Figure 4(a) and $M_{sw}/M_{sw0} = 1$ for Figure 4(b). Because larger planets have larger geothermal heat fluxes and thicker H_2O layers, these objects could have an internal ocean with a smaller H_2O mass on the planetary surface (Figure 4(a)) and a weaker initial radiogenic heat source (Figure 4(b)). However, larger planets also have larger gravitational accelerations. Thus, on those

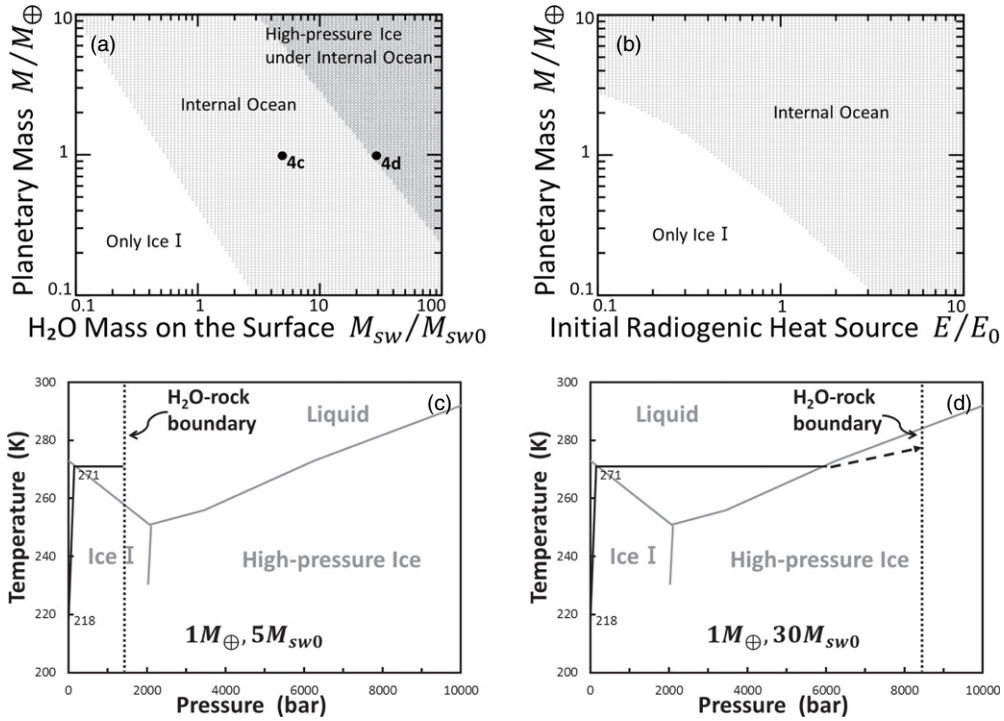

Figure 4. Surface conditions for a planet at 1 AU around a central star ($L = L_0$; the present luminosity of our Sun) and temperature profiles of surface H_2O layers for two cases. (a) The x axis is the surface H_2O mass and the y axis is planetary mass normalized by the Earth's mass, assuming $E/E_0 = 1$. The two dots in this panel indicate the conditions corresponding to the temperature profiles shown in panels (c) and (d). (b) The x axis is initial radiogenic heat, and the y axis is the planetary mass normalized by the Earth's mass, assuming $M_{sw}/M_{sw0} = 1$. (c) Temperature profile at 1 $M_\oplus$ and 5 M_{sw0}. (d) Temperature profile at 1 $M_\oplus$ and 30 M_{sw0}.

planets, high-pressure ice tends to appear under the internal ocean with a smaller H_2O mass on the surface (Figure 4(a)). For example, if a planet of mass 1 $M_\oplus$ has an H_2O mass of 0.6 $M_\oplus$–25 M_{sw0}, it could have an internal ocean. However, if a planet has an H_2O mass $> 25\,M_{sw0}$, high-pressure ice should exist under the ocean (Figure 4(a)). Note, however, that an internal ocean can exist on a planet having a mass of 1 $M_\oplus$ if the initial radiogenic heat source exceeds $0.4E_0$ (Figure 4(b)). Figures 4(c) and (d) show the temperature profiles of surface H_2O layers. Figure 4(c) shows the conditions of a planet parameterized by 1 $M_\oplus$ and 5 M_{sw0}, whereas Figure 4(d) shows the conditions of a planet parameterized by 1 $M_\oplus$ and 30 M_{sw0}. Given the conditions of Figure 4(c), the surface H_2O layers consist of a conductive-ice Ih layer and a convective liquid layer (i.e., an internal ocean). When the planet has a higher H_2O mass, high-pressure ice could appear under the internal ocean (Figure 4(d)). Here, the planetary surface temperature seems very low, so we assume that the planet is covered by ice that has a higher albedo (∼0.6) than ocean/land (∼0.3).

Figures 5(a) and (b) show the surface conditions for free-floating planets ($L = 0$) with masses from 0.1 $M_\oplus$ to 10 $M_\oplus$ 4.6 billion yr after planetary formation. The incident flux from the central star affects the surface temperature, thereby affecting the condition on the surface. Therefore, the conditions, and in particular those shown in Figure 5(a), are different from those shown in Figures 4(a) and (b). The results of Figure 5(a) show that, regardless of the amount of H_2O a 1 $M_\oplus$ planet has, an internal ocean cannot exist under the ice shell. An internal ocean could exist on free-floating planets under certain conditions, but the planetary size and water abundance strongly constrain these conditions (see Figure 5(a)). For instance, if a free-floating planet has an initial radiogenic heat source greater than $7E_0$, it can have an internal ocean (Figure 5(b)). Figures 5(c) and (d) show the temperature gradients of surface H_2O layers for free-floating planets. The parameters are set to the same values as those in Figures 4(c) and (b), except that $L = 0$. The temperature on the planetary surface, approximately 35 K, is calculated by Equation (6) under the assumption that $L = 0$ and the ice Ih layer is thicker than that for the conditions of Figures 4(c) and (d). Given the conditions of Figure 5(c), the surface H_2O layers consist only of a conductive ice Ih layer. However, for higher H_2O mass, high-pressure ice could appear under the ice Ih layer (Figure 5(d)).

Figure 6 shows the surface conditions for planets with masses from 0.1 $M_\oplus$ to 10 $M_\oplus$ at varying distances from a central star, 4.6 billion yr after planetary formation. The runaway greenhouse limit (Kasting 1988; Nakajima et al. 1992) indicating the inner edge of the HZ is not considered. The effect of the incident flux from the central star on the surface conditions is estimated in each graph of Figure 6 as a function of distance from the central star. We find that the existence of an internal ocean on planets far from a central star depends on the planetary mass and surface H_2O mass. For the conditions of Figure 6(b) on which a planet has two times the H_2O mass (i.e., 2 M_{sw}/M_{sw0}), for example, a 2 $M_\oplus$ planet can have an internal ocean under which there is no high-pressure ice only out to approximately 7 AU from the central star. For a planet with five times the H_2O mass (i.e., 5 M_{sw}/M_{sw0}; Figure 6(c)), an internal ocean with no underlying high-pressure ice can exist out to approximately 30 AU. However, if the planet has 10 times the H_2O mass (i.e., 10 M_{sw}/M_{sw0}; Figure 6(d)), an internal ocean without underlying high-pressure ice could exist to only approximately 5 AU. The planetary mass and surface H_2O mass strongly constrain the conditions under which an extrasolar terrestrial planet far from its central star can have an internal ocean with no underlying high-pressure ice.

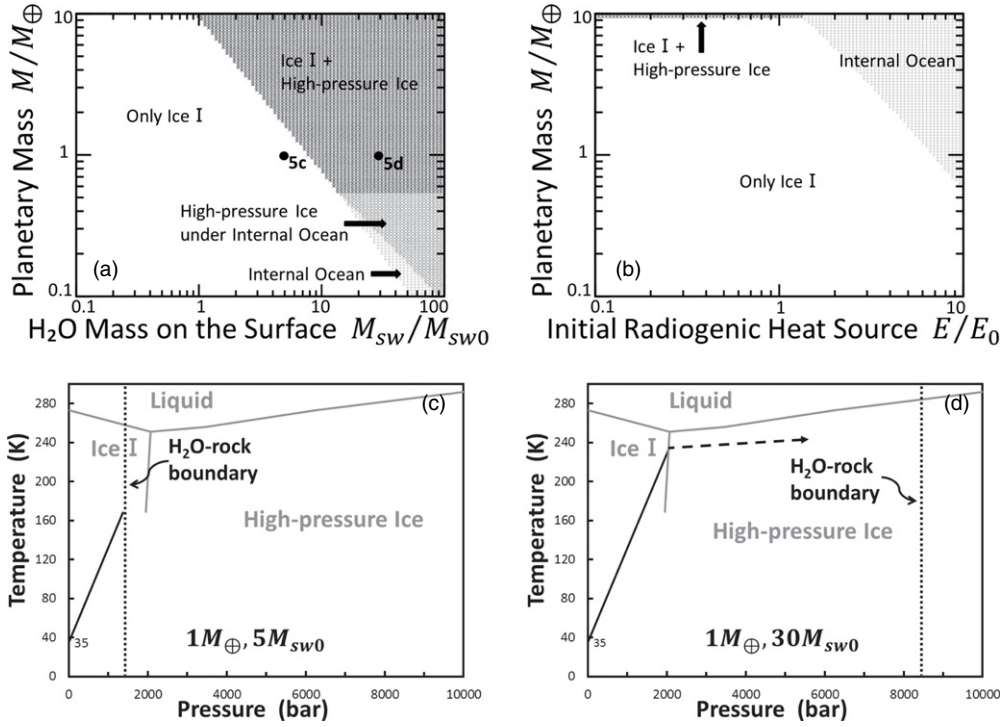

Figure 5. Same as Figure 4, but for a free-floating planet ($L = 0$).

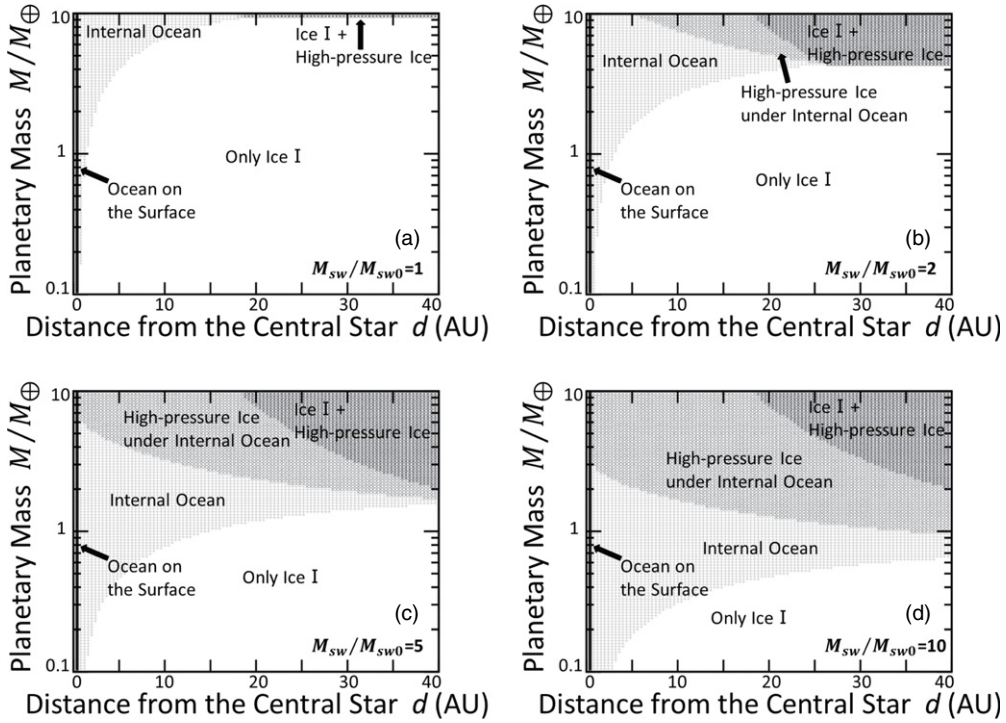

Figure 6. Conditions for a planet orbiting central star ($E/E_0 = 1$) for (a) $M_{sw}/M_{sw0} = 1$, (b) $M_{sw}/M_{sw0} = 2$, (c) $M_{sw}/M_{sw0} = 5$, and (d) $M_{sw}/M_{sw0} = 10$. The x axes represent the distance from the central star and the y axes represent the planetary mass normalized by Earth's mass.

4. DISCUSSION

4.1. Models of Study

We expanded on the models of Tajika (2008) by (1) invoking the mass–radius relationship (Equation (1)) to consider planetary compression by gravity, (2) considering the temperature dependence of the thermal conductivity of ice Ih (Equation (4)), and varying the (3) abundance of radiogenic heat sources and (4) H_2O abundance on the surface, both of which were held constant in Tajika (2008). We used Equation (1) to determine the mass–radius relationships because we expected more accurate results, although this change makes little quantitative difference in the results. Below, we discuss items (2), (3), and (4) to analyze the models of this study.

It is known from experiments that the thermal conductivity of ice Ih depends on temperature ($\approx 1/T$; Klinger 1980). In the

present study, the surface ice shell is thicker than that considered by Tajika (2008). For example, the surface ice shell considered herein is about 1.1 times thicker at 1 AU and about 3.5–4.4 times thicker on the free-floating planets ($L = 0$). This increased thickness is due to the use of Equation (4) to describe the thermal conductivity of ice Ih in contrast with Tajika (2008), where a constant thermal conductivity ($k_i = 2.2$) was used. Tajika (2008) treated the abundance of H_2O and heat source elements (a ratio of mass against a planetary mass) as a constant, i.e., $M_{sw}/M_{sw0} = 1$ ($M_{sw0} = 0.00023M$) and $E/E_0 = 1$, although the amounts should vary with planetary mass, and showed that liquid water would be stable either on the surface or beneath the ice for a planet with a mass exceeding $4\,M_\oplus$, regardless of the planetary orbit and the luminosity of the central star. In this paper, however, when we consider a planet with parameters $M_{sw}/M_{sw0} = 1$ and $E/E_0 = 1$, the results shown in Figure 5 are not consistent with those of Tajika (2008). Our results indicate that free-floating planets with masses between $0.1\,M_\oplus$ and $10\,M_\oplus$ could not have liquid water on their surfaces and also under the ice for the planetary parameters $M_{sw}/M_{sw0} = 1$ and $E/E_0 = 1$. As explained, when using Equation (4) to describe the thermal conductivity of ice Ih, the planetary surface temperature becomes more sensitive to the thickness of the surface ice layer, which leads to a several-times increase in the thickness of the surface ice. These results thus differ from those of Tajika (2008).

In this study, we assume that the high-pressure layer continues to the H_2O–rock boundary from the point where the temperature–pressure line crosses into the high-pressure ice part (see Section 2.2). The results of this paper could depend on this assumption. When the thermal conductivity of high-pressure ice is comparatively low (similar to that of ice Ih), the heat cannot be effectively transported through the high-pressure ice, thus the bottom of the high-pressure ice could be thermally unstable and melt enough to form an internal ocean.

The results of the present study indicate that the high-pressure layers under an internal ocean could be from $\lesssim$1 km to $\sim$100 km thick because a super-Earth planet characterized by a few percent H_2O by weight could have $\sim$100 km thick high-pressure ice layers. In high-pressure ice that is $\sim$100 km thick, it is possible for convective ice layers to appear. To estimate whether or not such convection layers arise, we use the Rayleigh number R_a, which is given by

$$R_a = \frac{g\alpha\rho a^3 \Delta T}{\kappa\eta}, \tag{10}$$

where α is the coefficient of thermal expansion, ρ is the density, a is the thickness of the high-pressure ice layer, ΔT is the temperature difference between the top and bottom part of the layer, κ is the thermal diffusivity, and η is the viscosity coefficient. When the Rayleigh number R_a exceeds the critical value for the onset of convection ($R_{a_{\rm crit}} \sim 10^3$), convective motion spontaneously begins. If we use the parameters from Kubo (2008), i.e., $\alpha = 10^{-4}$ K^{-1}, $\rho = 1000$ kg m^{-3}, $\Delta T = 50$ K, $\kappa = 2 \times 10^{-6}$ m^2 s^{-1}, and $\eta = 10^{15}$–10^{18} Pa s and the typical values from this study, $g = 10$ m s^{-2} and $a = 10^2$ km, the Rayleigh number is $\sim 10^4$–10^7, which indicates that convective motion is possible.

In this study, we consider M_{sw} from 0.1 M_{sw0} (0.0023% by weight) to 100 M_{sw0} (2.3% by weight). If the planet has significantly more H_2O on its surface, the water layer would be very thick and our model would not apply. If the planet has significantly less H_2O on its surface, the regassing flux of water would change because of insufficient water on the surface and the planet's thermal evolution would differ from that of the Earth. In other words, we consider only those planets that are relatively active geothermally and have a comparable amount of water as Earth-like planets. Improving our model so that it applies to other types of terrestrial planets is an important problem that we leave for future work.

4.2. Habitability of an Internal Ocean

For genesis and sustenance of life, we need at least (1) liquid water and (2) nutrient salts because these substances are required to synthesize the body of life (Maruyama et al. 2013). Because nutrient salts are supplied from rocks, it is necessary that liquid water be in contact with rock to liberate the salts. A type 5 planet (Figure 3(b)) is thus not likely to be habitable because the internal ocean does not come in contract with rocks. However, it is possible for a type 2 planet to meet this requirement. Therefore, we presume that only type 2 planets have an internal ocean that is possibly habitable.

Therefore, the results of this study indicate that planetary mass and H_2O mass constitute two more conditions to add to the previous conditions for an extrasolar planet to have an internal ocean without high-pressure ice. In other words, these considerations indicate that only a planet with the appropriate planetary mass and H_2O mass can have an internal ocean that is possibly habitable.

However, it is possible that hydrothermal activities within the rocky crust may transfer nutrient salts to the internal ocean through cracks in the high-pressure ice. Large terrestrial planets such as those considered in this study are likely to have areas of high geothermal activity along mid-oceanic ridges and subduction zones as well as large submarine volcanos whose tops might emerge into the internal ocean from the high-pressure ice. Furthermore, for planets with thick, high-pressure ice layers (Section 4.1), the convective ice layer could transfer nutrient salts from the rock to the internal ocean. In these cases, high-pressure ice might not prevent the nutrient flux from the rock floor from reaching the internal ocean.

4.3. Future Work

As shown in Figures 4(b) and 5(b), an appropriate initial radiogenic heat source is an important factor in determining whether or not a planet has an internal ocean. Because the variation in the amount of initial heat generation in planets throughout space is not known, we assume in this study that the initial heat generation E per unit time and volume ranges from $0.1E_0$ to $10E_0$. Thus, in order to resolve this issue, the general amount of radiogenic heat sources for extrasolar terrestrial planets should be estimated.

An Earth-size planet ($M_{sw}/M_{sw0} = 1$, $E/E_0 = 1$) orbiting at 1 AU around the Sun for 4.6 billion yr with no greenhouse gases might be globally covered by ice (Figure 4). In contrast, the Earth is currently partially covered with ice but retains liquid water on its surface. Therefore, it is almost certain that greenhouse gases play a major role in keeping the surface warm. Even free-floating, Earth-sized planets with atmospheres rich in molecular hydrogen could have liquid water on their surfaces because geothermal heat from their interiors would be retained due to the greenhouse gas effect of H_2 (Stevenson 1999). By applying this model here, we can account for the greenhouse gas effect for various values of the emissivity ε in Equation (6). In future work, we will thus discuss how greenhouse gases modify the

conditions necessary for the development of a terrestrial ocean planet or ice-covered planet with an internal ocean.

In the present study, we assumed pure H_2O on the planetary surface. However, even if an extrasolar terrestrial planet has surface H_2O, the H_2O might not be pure because it might contain dissolved nutrient salts such as those found in Earth's oceans. In this case, the melting point of the solution would differ from that of pure H_2O. Moreover, the phase diagram would become more complicated and the properties of H_2O (e.g., its thermal conductivity) could be transmuted as a result of the appearance of phases in which H_2O ice contains nutrient salts. A very important work would thus be to analyze multicomponent water (e.g., seawater on Earth) to see what qualitative changes such a modified phase diagram would bring to our results.

Consider the examples Europa and Ganymede, which are two satellites of Jupiter and are thought to have internal oceans. Ganymede is thought to have high-pressure ice under its internal ocean (see, e.g., Lupo 1982). Therefore, determining whether the internal oceans of Europa and Ganymede are suitable for life would be pertinent to the discussion of the habitability of internal oceans with or without high-pressure ice. In addition, a more circumstantial discussion of the habitability of internal oceans would require considering the redox gradient within the internal ocean (as exemplified by the discussions of Europa Gaidos et al. 1999) and the effects of the riverine flux of nutrient salts (Maruyama et al. 2013).

5. CONCLUSIONS

Herein, we discuss the conditions that must be satisfied for ice-covered bound and unbound terrestrial planets to have an internal ocean on the timescale of planetary evolution. Geothermal heat flow from the planetary interior is considered as the heat source at the origin of the internal ocean. By applying and improving the model of Tajika (2008), we also examine how the amount of radiogenic heat and H_2O mass affect these conditions. Moreover, we investigate the structures of surface H_2O layers of snowball planets by considering the effects of high-pressure ice. The results indicate that planetary mass and surface H_2O mass strongly constrain the conditions under which an extrasolar terrestrial planet might have an internal ocean without high-pressure ice existing under the internal ocean.

We thank the reviewer Eiichi Tajika for constructive comments. We also thank S. Ida and M. Ikoma for valuable discussions. This research was supported by a grant for the Global COE Program "From the Earth to 'Earths' " from the Ministry of Education, Culture, Sports, Science, and Technology of Japan. T.S. was supported by a Grant-in-Aid for Young Scientists (B), JSPS KAKENHI grant No. 24740120.

APPENDIX

PARAMETERIZED CONVECTION MODEL

By applying conservation of energy, we obtain

$$4\pi R_m^2 q + \frac{4}{3}\pi\rho c\left(R_m^3 - R_c^3\right)\frac{dT_m}{dt} = \frac{4}{3}\pi E(t)\left(R_m^3 - R_c^3\right), \tag{A1}$$

where ρ is the density of the mantle, c is the specific heat at constant pressure, R_m and R_c are the outer and inner radii of the mantle, respectively, T_m is the average mantle temperature, and $E(t)$ is the rate of energy production by decay of radiogenic heat sources in the mantle per unit volume.

The mantle heat flux is parameterized in terms of the Rayleigh number R_a as

$$q = \frac{k(T_m - T')}{R_m - R_c}\left(\frac{R_a}{R_{a_{\rm crit}}}\right)^{\beta}, \tag{A2}$$

where k is the thermal conductivity of the mantle, T' is the temperature at the surface of the mantle, $R_{a_{\rm crit}}$ is the critical value of R_a for convection onset, and β is an empirical constant.

The radiogenic heat source is parameterized as

$$E(t) = Ee^{-\lambda t}, \tag{A3}$$

where λ is the decay constant of the radiogenic heat source and E is the initial heat generation per unit time and volume. We assume E to range between $0.1E_0$–$10E_0$, where the constant E_0 is the initial heat generation estimated from the present heat flux of the Earth.

We obtain R_a as

$$R_a = \frac{g\alpha(T_m - T')(R_m - R_c)^3}{\kappa\nu}, \tag{A4}$$

where α is the coefficient of thermal expansion, κ is the thermal diffusivity, and ν is the water-dependent kinematic viscosity. The viscosity ν strongly depends on the evolution of the mass M_w of mantle water and the mantle temperature T_m and is parameterized as

$$\nu = \nu_m \exp(T_A/T_m), \tag{A5}$$

$$T_A = \alpha_1 + \alpha_2 x, \tag{A6}$$

$$x = \frac{M_w}{M_m}, \tag{A7}$$

where ν_m, α_1, and α_2 are constants, T_A is the activation temperature for solid-state creep, and M_m is the mass of the mantle.

The evolution of the mantle water can be described by the regassing flux $F_{\rm reg}$ and outgassing flux $F_{\rm out}$ as

$$\begin{aligned}\frac{dM_w}{dt} &= F_{\rm reg} - F_{\rm out}\\ &= f_{\rm bas}\rho_{\rm bas}d_{\rm bas}SR_{\rm H_2O} - \frac{M_w}{\frac{4}{3}\pi\left(R_m^3 - R_c^3\right)}d_m f_w S,\end{aligned} \tag{A8}$$

where $f_{\rm bas}$ is the water content in the basalt layer, $\rho_{\rm bas}$ is the average density, $d_{\rm bas}$ is the average thickness of the basalt layer before subduction, S is the areal spreading rate, $R_{\rm H_2O}$ is the regassing ratio of water, d_m is the melting generation depth, and f_w is the outgassing fraction of water. The regassing ratio of water linearly depends on the mean mantle temperature T_m via

$$R_{\rm H_2O} = R_T(T_m(0) - T_m) + R_{\rm H_2O,0}, \tag{A9}$$

as given by von Bloh et al. (2007), where R_T is the temperature dependence of the regassing ratio and $R_{\rm H_2O,0}$ is the initial regassing ratio. The areal spreading rate S is

$$S = \frac{q^2\pi\kappa A_0}{4k^2(T_m - T')^2}, \tag{A10}$$

Table 1
Values of the Parameter for Parameterized Convection Model

Parameter	Value	Unit	Source
$R_m(1\,M_\oplus)$	$6{,}271 \times 10^3$	m	von Bloh et al. (2007)
$R_c(1\,M_\oplus)$	$3{,}471 \times 10^3$	m	von Bloh et al. (2007)
ρc	4.2×10^6	J m^{-3} K^{-1}	von Bloh et al. (2007)
$T_m(0)$	3,000	K	von Bloh et al. (2007)
k	4.2	J s^{-1} m^{-1} K^{-1}	von Bloh et al. (2007)
$R_{a_{\rm crit}}$	1,100		von Bloh et al. (2007)
β	0.3		von Bloh et al. (2007)
E_0	1.46×10^{-7}	J s^{-1}m^{-3}	von Bloh et al. (2007)
λ	0.34	Gyr^{-1}	von Bloh et al. (2007)
$g(1\,M_\oplus)$	9.81	m s^{-2}	von Bloh et al. (2007)
α	3×10^{-5}	K^{-1}	von Bloh et al. (2007)
κ	10^{-6}	m^2 s^{-1}	von Bloh et al. (2007)
ν_m	2.21×10^{-7}	m^2 s^{-1}	McGovern & Schubert (1989)
α_1	6.4×10^4	K	Franck & Bounama (1995)
α_2	-6.1×10^6	K per weight fraction	Franck & Bounama (1995)
$M_m(1\,M_\oplus)$	4.06×10^{24}	kg	Franck & Bounama (1995)
$M_w(0)(1\,M_\oplus)$	4.2×10^{21}	kg	von Bloh et al. (2007)
$f_{\rm bas}$	0.03		von Bloh et al. (2007)
$\rho_{\rm bas}$	2,950	kg m^{-3}	von Bloh et al. (2007)
$d_{\rm bas}$	5×10^3	m	von Bloh et al. (2007)
d_m	40×10^3	m	von Bloh et al. (2007)
f_w	0.194		von Bloh et al. (2007)
R_T	29.8×10^{-5}	K^{-1}	von Bloh et al. (2007)
$R_{\rm H_2O,0}$	0.001		von Bloh et al. (2007)
A_0^*	3.1×10^{14}	m^2	McGovern & Schubert (1989)

where A_0 is the ocean basin area. The area A_0 can be parameterized as

$$\frac{A_0}{A_0^*} = \left(\frac{R}{R_\oplus}\right)^2, \tag{A11}$$

where A_0^* is the present ocean basin area on Earth. By using Equation (1), we obtain

$$A_0 = A_0^* \left(\frac{M}{M_\oplus}\right)^{0.54}. \tag{A12}$$

In Table 1, we summarize selected values for the parameters used in the parameterized convection model.

REFERENCES

Budyko, M. I. 1969, Tell, 21, 611
Franck, S., & Bounama, C. 1995, PEPI, 92, 57
Gaidos, E. J., Nealson, K. H., & Kirschvink, J. L. 1999, Sci, 284, 1631
Genda, H., & Ikoma, M. 2008, Icar, 194, 42
Gough, D. O. 1981, SoPh, 74, 21
Hart, M. H. 1979, Icar, 37, 351
Hoffman, P. F., Kaufman, A. J., Halverson, G. P., & Schrag, D. P. 1998, Sci, 281, 1342
Hoffman, P. F., & Schrag, D. P. 2002, Terra Nova, 14, 129
Howard, A. W., Marcy, G. W., Johnson, J. A., et al. 2010, Sci, 330, 653
Kamb, B. 1973, in Physics and Chemistry of Ice, ed. E. Whalley, S. J. Jones, & L. W. Gold (Ottawa: Royal Society of Canada), 28
Kasting, J. F. 1988, Icar, 74, 472
Kasting, J. F., Whitmire, D. P., & Reynolds, R. T. 1993, Icar, 101, 108
Klinger, J. 1975, JGlac, 14, 517
Klinger, J. 1980, Sci, 209, 271
Kubo, T. 2008, Low Temp. Sci, 66, 123
Lupo, M. J. 1982, Icar, 52, 40
Maruyama, S., Ikoma, M., Genda, H., et al. 2013, Geoscience Frontiers, 4, 141
Mayor, M., & Queloz, D. 1995, Natur, 378, 355
McGovern, P. J., & Schubert, G. 1989, E&PSL, 96, 27
Mischna, M. A., Kasting, J. F., Pavlov, A., & Freedman, R. 2000, Icar, 145, 546
Nakajima, S., Hayashi, Y.-Y., & Abe, Y. 1992, JAtS, 49, 2256
Sellers, W. D. 1969, JApMe, 8, 392
Stevenson, D. J. 1999, Natur, 400, 32
Sumi, T., Kamiya, K., Bennett, D. P., et al. 2011, Natur, 473, 349
Tajika, E. 2008, ApJL, 680, L53
Tajika, E., & Matsui, T. 1992, E&PSL, 113, 251
Valencia, D., O'Connell, R. J., & Sasselov, D. 2006, Icar, 181, 545
Varrot, M., Rochas, G., & Klinger, J. 1978, JGlac, 21, 241
von Bloh, W., Bounama, C., Cuntz, M., & Franck, S. 2007, A&A, 476, 1365